Loss of caveolin-3 induced by the dystrophy-associated P104L mutation impairs L-type calcium channel function in mouse skeletal muscle cells.

Harold Couchoux, Bruno Allard, Claude Legrand, Vincent Jacquemond, Christine Berthier

Loss of caveolin-3 induced by the dystrophy-associated P104L mutation impairs L-type calcium channel function in mouse skeletal muscle cells

Harold Couchoux, Bruno Allard, Claude Legrand, Vincent Jacquemond and Christine Berthier

Université Lyon 1, CNRS, Physiologie Intégrative, Cellulaire et Moléculaire, Villeurbanne, F-69622, France.

Corresponding author: Christine Berthier (email: christine.berthier@univ-lyon1.fr)

Running title: Caveolin-3 modulates L-type Ca^{2+} channel function and localization

Key words: L-type calcium channel, caveolin, skeletal muscle

Total number of words: 6 974

Abstract

Caveolins are membrane scaffolding proteins which associate with- and regulate a variety of signalling proteins, including ion channels. A deficiency in caveolin-3 (Cav-3), the major striated muscle isoform, is responsible for skeletal muscle disorders, such as limb girdle muscular dystrophy 1C (LGMD 1C). The molecular mechanisms leading to the muscle wasting that characterizes this pathology are poorly understood. Here we show that a loss of Cav-3 induced by the expression of the LGMD 1C-associated mutant P104L (Cav-3^{P104L}) provokes a reduction by half of the maximal conductance of the voltage-dependent L-type Ca^{2+} channel in mouse primary cultured myotubes and foetal skeletal muscle fibers. Confocal immunomiscrocopy indicated a colocalization of Cav-3 and $Ca_v1.1$, the pore-forming subunit of the L-type Ca^{2+} channel, at the surface membrane and in the developing T-tubule network in control myotubes and foetal fibers. In myotubes expressing Cav-3^{P104L}, the loss of Cav-3 was accompanied by a 66% reduction in $Ca_v1.1$ mean labelling intensity. Our results suggest that Cav-3 is involved in proper L-type Ca^{2+} channel membrane function and localization in skeletal muscle cells and that an alteration of L-type Ca^{2+} channels could be involved in the physiopathological mechanisms of caveolinopathies.

Introduction

Caveolins are integral membrane proteins associated with cholesterol-rich omega-shaped plasma membrane pits called caveolae (Parton & Richards, 2003; Cohen *et al.* 2004). The mammalian caveolin protein family comprises caveolin-1 and -2, expressed in many non-muscle cells and the muscle-specific caveolin-3 (Cav-3) (Way & Parton, 1995; Tang *et al.* 1996). In the recent years, point mutations and deletions in the human *CAV3* gene were shown to be responsible for several muscle disorders (Cohen *et al.* 2004; Fulizio *et al.* 2005). One of the best characterized mutation consists in the P104L substitution, associated with limb girdle muscular dystrophy 1C (LGMD 1C) (Minetti *et al.* 1998; Betz *et al.* 2001). Cav-3^{P104L} exerts a dominant negative effect presumably through the formation of aggregates with the wild type Cav-3 which accumulate in the Golgi complex and are degraded through a proteasome-dependent mechanism (Galbiati *et al.* 1999a; Galbiati *et al.* 1999b; Sunada *et al.* 2001; Carozzi *et al.* 2002).

How a defective Cav-3 expression leads to muscle disorders remains very mysterious, largely due to the poor understanding of the role played by Cav-3 in normal skeletal muscle function and to controversial related series of results described in the literature. Results obtained using antisense inhibition of Cav-3 expression in cultured C2C12 skeletal muscle cells suggest a role for Cav-3 in promoting myoblast fusion (Galbiati *et al.* 1999a) whereas opposite conclusions were drawn from results obtained on muscle cell lines derived from *Cav-3* null mice and Cav-3 over-expressing mice (Volonte *et al.* 2003). Also, recent results obtained on zebrafish embryos after Cav-3 knock-down suggested that Cav-3 is required for correct muscle intracellular organization and myogenesis (Nixon *et al.* 2005). Along this line, immunolabeling experiments revealed a close association of Cav-3 with the T-tubule network in developing and mature skeletal muscle fibers (Parton *et al.* 1997; Galbiati *et al.* 2001; Ralston and Ploug, 1999). Additionally, T-tubule structure was shown to be altered in Cav-3 deficient muscles suggesting that the protein may play a role in proper T-tubule network organization (Galbiati *et al.* 2001; Minetti *et al.* 2002).

Although multiple molecular investigations have shown that Cav-3 may associate with a number of structural or signalling proteins including dystroglycan (Song *et al.* 1996; Sotgia *et al.* 2000), M-phosphofructokinase (Scherer & Lisanti, 1997), dysferlin (Matsuda *et al.* 2001) or nitric oxide synthase (Feron *et al.* 1996; Venema *et al.* 1997), there is still no explanation as to how Cav-3 deficiency leads to the progressive and irreversible skeletal muscle wasting that characterizes muscular caveolinopathies. Alteration of intracellular Ca^{2+} handling is the source of various cell disorders and is highly suspected to be involved in a number of the most devastating degenerative muscle pathologies (Mallouk *et al.* 2000; Rizzuto & Pozzan, 2003). Yet, up to now, the consequences of a down-regulation of Cav-3 on skeletal muscle Ca^{2+} homeostasis have never been investigated. Interestingly we previously showed that depletion of membrane cholesterol in foetal skeletal fibers induced a disruption of caveolae and T-tubules and a marked reduction in the L-type Ca^{2+} channel function of the dihydropyridine receptor (DHPR), a critical element in the regulation of intracellular Ca^{2+} in skeletal muscle (Pouvreau *et al.* 2004a). This altered L-type voltage-dependent Ca^{2+} channel function caused by cholesterol depletion could have resulted from the associated loss of Cav-3.

Here, we investigated the properties of voltage-dependent Ca^{2+} channels in mouse primary cultured myotubes and in foetal muscle fibers expressing the LGMD 1C-associated Cav-3^{P104L} mutant.

We demonstrate that the loss of Cav-3 induced by expression of the Cav-3^{P104L} mutant induces (i) a drastic reduction in the maximum conductance of the voltage-activated L-type Ca^{2+} channel in both models, and (ii) a decrease in the labelling intensity of the pore-forming alpha1S subunit of the DHPR protein ($Ca_v1.1$).

Part of this work has been published in abstract form (Couchoux *et al.* 2006).

Methods

All experiments were carried out at room temperature unless otherwise stated.

Isolation and culture of skeletal muscle cells

A suspension of muscle cells was first obtained from ribcages of 18-day-old mouse foetuses (Swiss OF1, Charles River, France) using enzymatic treatment, as previously described (Pouvreau *et al.* 2004a). Briefly, pregnant mice were killed by cervical dislocation and the foetuses were extracted after laparotomy and killed by decapitation, in accordance with local ethical guidelines laid down by the French directives for care of laboratory animals (decree 87–848). The two halves of the ribcage of each foetus were dissected in normal Tyrode solution containing (mM): 140 NaCl, 5 KCl, 2.5 $CaCl_2$, 1 $MgCl_2$, 10 Hepes-NaOH, pH 7.4. The tissues were incubated at 37 °C for 15 min in normal Tyrode solution containing 3 mg ml^{-1} collagenase (type I, Sigma) and 1 mg ml^{-1} trypsin (type III, Sigma). Fibers were isolated by trituration with a sterile pipette and then allowed to sediment for 10 min–according to a procedure described by Rahkila and collaborators (Rahkila *et al.* 1996), plated on poly-D-lysine-coated dishes and cultured in survival medium (DMEM with 2% decomplemented horse serum).

For primary cultured skeletal myotubes, the supernatant from the sedimentation step was twice dispersed in dishes coated with calf skin collagens (Calbiochem) and allowed to sediment for 15 min to remove fibroblasts. Myoblasts from the supernatant were grown in proliferation medium consisting of DMEM with 10% foetal bovine serum, 10% horse serum and 2% chick embryo extract until transfection. All cells were cultivated at 37°C in 5% CO2.

Transfection

Plasmids encoding YFP-tagged wild type Cav-3 (Cav-3^{wt} -YFP) and HA-tagged Cav-3^{P104L} were generously provided by R. Parton (University of Queensland, Australia). YFP-tagged Cav-3^{P104L} (Cav-3^{P104L}-YFP) was generated by subcloning into pEYFP (Clontech) using Kpn I/BamHI restriction sites.

Foetal fibers were transfected after 2 days in survival conditions using CombiMag (OzBiosciences) combined with FuGene 6 (Roche Diagnostics). Primary myoblasts were transfected at ~70% confluency using the same method and were allowed subsequently to differentiate by switching to DMEM with 10% foetal bovine serum. Immunostaining and electrophysiology experiments were performed 5 days post-transfection.

Immunofluorescence staining

Cells were fixed with 1% paraformaldehyde-0.01% glutaraldehyde in PBS (10 minutes) and permeabilized with 1% Triton X100-50 mM glycine in PBS (5 minutes). Non-specific sites were blocked with 3% normal goat serum (NGS)-0.1% bovine serum albumin in PBS (30 minutes) and endogenous biotins were saturated using the Avidin/Biotin Blocking kit (Vector Laboratories). Cells were then incubated for 2 hours with anti-Cav-3 rabbit polyclonal antibody (PA1-066, Affinity BioReagents) or anti-$Ca_v1.1$ mouse monoclonal antibody (mAb427, Chemicon International) diluted respectively 1:1,500 and 1:500 in PBS with 1% NGS. Cells were subsequently incubated for 30 minutes with biotin-conjugated goat anti-rabbit or goat anti-mouse IgG (Jackson Immunoresearch Laboratories) diluted 1:1,000 in PBS with 1% NGS and treated for 30 minutes with Cy3- or $Alexa_{488}$-conjugated streptavidin (Jackson Immunoresearch Laboratories or Molecular Probes, respectively) diluted 1:1,000 in PBS. For sequential labelling, cells were first labelled with the anti-Cav-3 primary antibody then labelled with the anti- $Ca_v1.1$ primary antibody after performing a mouse non specific sites blocking step (MOM Blocking kit, Vector Laboratories). Preparations were all mounted in anti-fading medium (Vectashield) and examined using a LSM 510 confocal fluorescence microscope (Zeiss). Excitation was performed with argon and helium/neon lasers at 488 or 533 nm and optical sections were collected using a 63x oil immersion objective and appropriate band pass filters.

Image Analysis

$Ca_v1.1$ labelling was quantified by numerical analysis of Z-series of confocal images taken from Cav-3^{P104L}-YFP transfected primary cultures after immunolabeling of

$Ca_v1.1$. The confocal Z-step size was set to 0.5 µm. Settings including photomultiplier gain, offset, aperture, and laser power were maintained rigorously identical to allow comparison of the labelling intensity between different samples.

Field-specific analysis was performed by measuring $Ca_v1.1$ immunoreactivity of Cav-3 ^{P104L}-YFP transfected myotubes and of non-transfected control myotubes present on a same RGB image. RGB images corresponding to each optical section of a given Z-stack were analyzed using the Image J software (National Institute of Health, Bethesda, MA, USA). Analysis was performed after extracting layers of each RGB image: the red layer corresponded to the Cav1.1 labelling (Cy3 image) and the green layer corresponded to the Cav-3^{P104L}-YFP signal. In order to quantify the labelling relative to the cell surface area, the cell outer limits had to be estimated from the fluorescence signals. In control myotubes this was achieved on the Cy3 image whereas in Cav-3^{P104L}-YFP transfected myotubes the Cav-3^{P104L}-YFP signal was used because of the very weak, unreliable $Ca_v1.1$ labelling in some of these myotubes. Non-labelled regions that clearly corresponded to nuclei were excluded from the area measurement.

Within the thus selected regions, the $Ca_v1.1$ immunoreactivity of Cav-3^{P104L}-YFP expressing myotubes and control myotubes was quantified on the Cy3 image by measuring the sum of the values of the pixels (integrated density) after optimally setting the threshold to eliminate background signal.

Mean $Ca_v1.1$ labelling intensity was determined for each control and transfected myotube present on a given image by normalizing the integrated density to the cell area. These measurements were performed on all images of the confocal stack and seven different stacks of images were analyzed.

Electrophysiology

Membrane currents were recorded in the whole cell configuration on cultured myotubes and foetal fibers using a patch clamp amplifier (RK 400, Bio-Logic). Pipettes were filled with (in mM): 110 Cs-aspartate, 20 TEACl, 2 $MgCl_2$, 5 MgATP, 10 EGTA, 10 HEPES, pH 7.2. The bath solution contained (in mM): 140 $TEAMeSO_3$, 10 $CaCl_2$, 2 $MgCl_2$, 0.001 TTX (Sigma), 10 HEPES, pH 7.2. Voltages were not corrected for liquid

junction potentials calculated to be less than 5 mV with the solutions used. Data acquisition and generation of command voltage pulses were done using the pClamp9 software driving the Digidata 1322A A/D, D/A converter (Axon Instruments Inc.). Cell capacitance, used to calculate the density of currents (A/F), was determined by integration of a control current trace obtained with a 10-mV depolarizing pulse from –80 mV. Leak currents were subtracted from all recordings using a 10-mV depolarizing pulse from the holding potential supposing a linear evolution of leak current with depolarization. The amplitude of the currents was measured at the peak of the currents and individual curves of the voltage dependence of $I_{Ca,\ L}$ density were fitted with the following equation (1): $I(V) = G_{max}(V-V_{rev})/\{1+exp[(V_{0.5}-V)/k]\}$, where $I(V)$ is the density of the current measured, V, the test pulse, G_{max}, the maximum conductance per capacitance, V_{rev}, the apparent reversal potential, $V_{0.5}$, the half-activation voltage, and k, a steepness factor. Individual curves of the voltage dependence of the normalized conductance were obtained by dividing $I(V)$ by $G_{max}(E - E_{rev})$.

Statistics

Non-linear least-squares fits were performed using a Marquadt-Levenberg algorithm routine included in Microcal Origin. Data values are presented as means ± S.E.M. In the figures, values of standard errors are in some cases smaller than data symbols and are therefore not apparent. Data were statistically analyzed using Student *t*-test. Values were considered significant when $P < 0.05$.

Results

Cav-3^{P104L} expression leads to the loss of endogenous Cav-3 in mouse primary cultured myotubes

We first examined Cav-3 imunolocalization in both control and Cav-3^{P104L}-expressing primary myotubes. The immunolabelling patterns shown on Fig. 1 are representative of results obtained in several independent experiments (n=5 for control and n=6 for Cav-3^{P104L}-transfected myotubes).

In control myotubes (Fig. 1A), Cav-3 labelling (red) was intense at the surface plasma membrane and was also characteristically present more discretely throughout the cell where it exhibited a punctate or reticular pattern consistent with the developing T-tubule membrane system (Flucher *et al.* 1991 ; Parton *et al*. 1997).

As shown in Fig. 1B, Cav-3^{P104L}-expressing myotubes displayed a different pattern of immunostaining (bottom panel). Yellow fluorescent protein (YFP)-tagged Cav-3^{P104L} (top panel) localized in perinuclear vesicles likely belonging to the Golgi apparatus. The corresponding Cav-3 labelling indicated that endogenous Cav-3 no longer reached the sarcolemma, being most often barely detectable (Fig. 1B). Our data thus confirm that expression of the mutant Cav-3^{P104L} in primary myotubes induces a drastic loss of endogenous membrane-associated Cav-3, as previously shown in adult skeletal muscle of transgenic mouse and LGMD-1C patients (Minetti *et al.* 1998; Sunada *et al.* 2001). Golgi-associated mutant or endogenous caveolin was not detected by the PA1-066 antibody, probably due to epitope-masking of the corresponding N-terminal epitope when in the Golgi compartment as previously suggested (Luetterforst *et al.* 1999).

The amplitude of the L-type Ca^{2+} current ($I_{Ca,\ L}$) is reduced in Cav-3^{P104L}-expressing mouse primary cultured myotubes

The properties of voltage-dependent Ca^{2+} channels were studied in control and Cav-3^{P104L}-expressing myotubes. Two types of voltage-dependent Ca^{2+} currents typical of cultured skeletal myotubes were recorded. $I_{Ca,\ T}$, displaying fast activating and inactivating kinetics, developed for depolarizations within the -40 to 0 mV range and $I_{Ca,\ L}$, displaying

slow activating and inactivating kinetics, was recorded for depolarizations to values more positive than –20 mV (Fig. 2A). We found that the amplitude of $I_{Ca,\,L}$ was strongly reduced in Cav-3^{P104L}-expressing myotubes as compared to control myotubes while $I_{Ca,\,T}$ remained unchanged (Figs 2A, B). For each cell, the current-voltage relationship of $I_{Ca,\,L}$ was fitted using equation 1 (see methods). Mean values for G_{max}, $V_{0.5}$, V_{rev} and k were 197 ± 12 S/F, 9 ± 0.8 mV, 65 ± 1.6 mV and 5 ± 0.4 mV for control myotubes (n = 40) and 88 ± 13 S/F, 11 ± 1.9 mV, 55 ± 2 mV and 5 ± 0.5 mV for Cav-3^{P104L}-expressing myotubes (n = 21), respectively (Fig. 2C). In Cav-3^{P104L}-expressing myotubes, there was a mean reduction of 55% of G_{max} and a 10 mV shift of V_{rev} towards negative potentials ($P < 0.0001$ and 0.001, respectively). The slight shift of E_{rev} was likely due to unmasking of a contaminating outward current component as a consequence of the decreased amplitude of the inward Ca^{2+} current. In myotubes transfected with YFP alone, G_{max} (191 ± 10, n = 6) was not significantly changed. Finally, we found that the mean capacitance was not significantly different in control myotubes (218 ± 20 pF, n = 40) and in Cav-3^{P104L}-expressing myotubes (229 ± 27 pF, n = 34).

Expression of Cav-3^{P104L} in myotubes alters the distribution and mean intensity of L-type voltage-dependent Ca^{2+} channel immunolabelling

A possible reason for the drastic reduction in the amplitude of $I_{Ca,\,L}$ induced by Cav-3^{P104L} expression is that loss of Cav-3 leads to a down-expression or defective targeting of the DHPR.

To explore this possibility, control and Cav-3^{P104L}-expressing myotubes were immunostained with anti-Cav-3 and anti- $Ca_v1.1$ antibodies. Representative images are shown on Figs 3 and 4. In control myotubes (Fig. 3) both proteins essentially colocalized, this being particularly apparent at the level of the surface plasma membrane. In the internal cellular compartment, such a colocalization is also visible although it appears more restricted to specific areas (arrowheads). The $Ca_v1.1$ labelling corresponded to an extended array of regularly distributed dots at the level of which Cav-3 labelling was, although not systematically, also concentrated. As for Fig.1, these labelled internal structures likely

belong to the nascent T-tubule system as previously documented (Flucher *et al.* 1991; Flucher *et al.* 1993; Parton *et al.* 1997).

In Cav-3^{P104L}-expressing myotubes, $Ca_v1.1$ labelling was clearly reduced (Fig. 4A). In addition, part of the residual labelling appeared to redistribute around the nuclei, likely within the Golgi compartment, as indicated by the colocalization with Cav-3^{P104L}-YFP (merged image).

$Ca_v1.1$ labelling intensity (mean pixel value per pixel of cell area) was measured in individual control and in Cav-3^{P104L}-expressing myotubes using numerical analysis of confocal images. As shown in Fig. 4B, the mean $Ca_v1.1$ labelling intensity in Cav3^{P104L}-expressing myotubes (23 ± 2.4 mean pixel value/pixel, n = 56) was significantly reduced by 66% as compared to control myotubes (68.2 ± 3.3, n = 134) ($P < 0.0001$). Comparing the labelling densities on pairs of control and Cav-3^{P104L}-expressing myotubes present in a same field image, so as to limit any bias introduced by variability within the different sampled images, yielded essentially identical results (not shown).

Cav-3^{P104L} expression in foetal skeletal muscle fibers also leads to the loss of endogenous Cav-3 and to a reduction of $I_{Ca,\,L}$ amplitude

Since Cav-3 is thought to be involved in muscle developmental processes, one of the possibilities is that the reduction of the voltage-dependent Ca^{2+} channel function in Cav-3^{P104L}-expressing cultured myotubes could result from abnormal myotube differentiation. To test for this, we explored the channel function in foetal skeletal muscle fibers maintained in survival conditions and transfected with YFP-tagged Cav-3^{P104L}. This cell system, although not fully mature, possesses a well differentiated skeletal muscle phenotype and is suitable for transfection.

As shown on Fig. 5A (top panel), Cav-3 immunolabeling was present at the level of both the surface and T-tubule membrane in the control fibers (cell on the right) while the labelling intensity was strongly decreased in the Cav-3^{P104L}-expressing foetal fibers (cell on the left) indicating that, as in cultured myotubes, expression of the mutant Cav-3^{P104L} induced an important loss of endogenous Cav-3. It is also worth noting that in foetal fibers Cav-3^{P104L}-YFP also accumulates perinuclearly. We then measured Ca^{2+} currents in Cav-

3^{P104L}-expressing foetal fibers. Under survival conditions, $I_{Ca,\,T}$ vanished after a few days in culture while robust $I_{Ca,\,L}$ could still be recorded (Fig. 5B, left and middle traces). This current was typical of foetal skeletal muscle fibers (Pouvreau *et al.* 2004a) with slow kinetics of activation, a threshold at –10 mV, a peak at +20 mV and a reversal potential close to +80 mV (Fig. 5C). Its amplitude was strongly decreased in Cav-3^{P104L}-expressing fibers as compared to control fibers. Mean values for G_{max}, $V_{0.5}$, V_{rev} and k were 203 ± 11 S/F, 10 ± 0.9 mV, 77 ± 1.1 mV and 4 ± 0.2 mV in control fibers (n = 31) and 85 ± 18 S/F, 16 ± 3.5 mV, 63 ± 5 mV and 4 ± 0.7 mV in Cav-3^{P104L}-expressing fibers (n = 8), respectively. G_{max} was significantly reduced by 58% ($P < 0.0001$) and V_{rev} and $V_{0.5}$ were significantly shifted by -14 mV *(*$P < 0.0001$*)* and +6 mV *(*$P < 0.02$*)* respectively, in Cav-3^{P104L}-expressing fibers as compared to control ones. The voltage shift of $V_{0.5}$ is clearly shown in the right panel of figure 5C, where the mean normalized conductance *versus* voltage relationship in control and Cav-3^{P104L} expressing foetal fibers is presented. Fitting the individual normalized conductance versus voltage relationship with a Boltzman equation gave mean values for $V_{0.5}$ and k of 12 ± 4.7 mV and 3.4 ± 2 mV in control fibers and of 17.7 ± 2.4 mV and 3.2 ± 0.6 mV in Cav-3^{P104L} expressing foetal fibers, respectively. The mean capacitance of Cav-3^{P104L}-expressing fibers (182 ± 13, n = 8) did not significantly differ from the one of control fibers (175 ± 21, n = 31).

Over-expression of wild type Cav-3 in foetal skeletal muscle fibers does not affect $I_{Ca,\,L}$

We also tested the effect of over-expression of wild type Cav-3 on the functional expression of the Ca^{2+} channels. For this, expression of an YFP-tagged wild type Cav-3 was achieved after transfection of foetal muscle fibers in survival conditions. Fig. 5A (bottom panel) shows that under these conditions YFP-tagged wild type Cav-3 appears concentrated at the surface plasma membrane as well as in discrete intracellular clusters presumably corresponding to T-tubules. The measured $I_{Ca,\,L}$ yielded similar properties in Cav-3 over-expressing fibers and in control ones (Figs 5B, C). Mean values for the parameters fitted from the individual I/V curves in Cav-3 over-expressing fibers were 188 ± 16 S/F, 8 ± 1.6 mV, 72 ± 1.4 mV and 4 ± 0.3 mV for G_{max}, $V_{0.5}$, V_{rev} and k respectively (n =

16). The only difference as compared to the control fibers was a slight 5 mV shift of V_{rev} towards negative potentials (P = 0.01).

Discussion

The present study demonstrates that expression of the LGMD-1C associated Cav-3^{P104L} mutant in skeletal muscle cells induces a very significant alteration of both the L-type voltage-dependent Ca^{2+} current and the cellular distribution of the corresponding channels in mouse skeletal muscle cells. Altogether, our results strongly suggest that a marked alteration of the function of the L-type voltage-dependent Ca^{2+} channel results from Cav-3 deficiency in skeletal muscle. Such a deficiency, revealed by an almost complete loss of immunolabeling, was induced here by the expression of Cav-3^{P104L} mutant in transfected primary cultured myotubes and foetal fibers, thereby reproducing the pathological loss of caveolin observed in skeletal muscle of LGMD-1C patients and transgenic mice bearing the P104L mutation (Minetti *et al.* 1998; Sunada *et al.* 2001). Upon expression of Cav-3^{P104L} in cultured myotubes and foetal fibers, mutant as well as of endogenous Cav-3 did not reach the sarcolemma and we observed a strong intracellular accumulation of Cav-3^{P104L}, presumably at the level of the Golgi apparatus, consistent with what was previously described in fibroblasts, C2C12, and LGMD-1C biopsies (Minetti *et al*. 1998; Galbiati *et al*.1999b; Carozzi *et al*. 2002).

The reduction of $I_{Ca,\ L}$ amplitude in $Cav3^{P104L}$-expressing myotubes (55%) was accompanied by a similar reduction in the $Ca_v1.1$ labelling intensity (66%). It is thus likely that the reduced $I_{Ca,\ L}$ mainly results from a reduced number of channels rather than from an alteration of the functional properties of the channel. It was recently suggested that Cav-3 is implicated in trafficking since its down-regulation was shown to lead to Golgi accumulation of dysferlin (Hernandez-Deviez *et al.* 2006). Trafficking and/or membrane-anchoring of channels such as store-operated Ca^{2+} channels were moreover found to be dependent on caveolin-1 (Brazer *et al.* 2003). In this respect, the partial Golgi redistribution of the $Ca_v1.1$ labelling and its marked reduction upon Cav-3^{P104L} expression suggests that Cav-3 may also act as a post Golgi trafficking partner for the DHPR. Cav-3 could exert such a role from the earliest stages of muscle differentiation since both proteins display similar temporal appearance patterns, as shown on cultured muscle cells. Several studies have indeed demonstrated that the mRNA and corresponding L-type voltage-dependent

Ca^{2+} channel protein appear at a detectable level as myoblasts fuse into myotubes (Romey *et al.* 1989; Varadi *et al.* 1989; Cognard *et al*. 1993; Kyselovic *et al.* 1994); likewise, Cav-3 expression was reported to be strongly induced upon differentiation of cultured mouse skeletal muscle cells (Way & Parton, 1995; Song *et al*. 1996; Tang *et al.* 1996; Parton *et al.* 1997).

Cav-3 is also believed to participate to skeletal muscle T-tubules biogenesis. This hypothesis first originated from ultrastuctural and immunofluorescence studies (Ishikawa, 1968; Franzini-Armstrong, 1991; Parton *et al.* 1997; Ralston & Ploug, 1999). Furthermore, skeletal muscles from Cav-3 knock-out mice and Cav-3^{P104L} expressing LGMD-1C patients were both reported to harbour T-tubule structure abnormalities, although not identical ones (Galbiati *et al.* 2001; Minetti *et al.* 2002). Although Cav-3 does not appear indispensable for the formation of the T-tubule network, these data suggest that Cav-3 may play a role in its proper organization. One possible hypothesis could thus be that the observed impairment of the DHPR Ca^{2+} channel function induced by $Cav3^{P104L}$-expression could result from an altered T-tubule biogenesis. In order to test this hypothesis, the mean electrical capacitance, which is a reliable index of the total membrane surface, was determined and found not significantly altered in Cav-3^{P104L}-expressing myotubes. This indicates that Cav-3^{P104L} expression did not alter the amount of the electrically active T-tubular membrane but rather specifically targeted the DHPR. This was further confirmed by results obtained in foetal muscle fibers in which a comparable decrease in maximal conductance of the L-type Ca^{2+} channel was observed upon Cav-3^{P104L} expression. Under these conditions, and in contrast to cultured myotubes, Cav-3^{P104L} expression was achieved at a maturation stage at which well formed T-tubules are already present (Takekura *et al.* 2001) so that an effect related to the disruption of T-tubules organization could hardly be raised. Besides, membrane capacitance was as well found unchanged in Cav-3^{P104L}-expressing foetal fibers. Furthermore, the lack of effect of Cav-3^{P104L} expression on $I_{Ca,\ T}$ in primary cultured myotubes provides a critical internal control in this set of experiments and further argues in favour of a selective effect of the loss of Cav-3 on DHPR.

Our immunolabeling experiments show that Cav-3 and DHPR proteins colocalize at both the surface and T-tubular membranes and are in agreement with previous studies

(Jorgensen *et al.* 1989; Parton *et al.* 1997; Ralston and Ploug, 1999). However, it is not entirely clear whether Cav-3 directly physically interacts with DHPR and/or indirectly serves to organize ion channel regulating molecules or membrane environment for proper ion channel targeting. A number of other ion channels have been shown to be specifically targeted to caveolin-rich microdomains in different tissues (Martens *et al.* 2004). In cardiac muscle, Cav-3 has been shown to coimmunoprecipitate with the cardiac isoform of the pore-forming subunit of the L-type Ca^{2+} channel and to play a role in the beta2-adrenergic response (Balijepalli *et al.* 2006). In endothelial cells, the Ca^{2+}-activated K^+ channel was found to directly interact with caveolin-1 (Wang *et al.* 2005) and caveolin-1 was also found to bind to the store-operated Ca^{2+} TRPC1 channels (Brazer *et al.* 2003). In our study, no reliable quantitative comparison of the $Ca_v1.1$ labelling between control and Cav-3^{P104L}-expressing foetal fibers could be achieved, due to the much lower transfection efficiency in this system. We thus cannot rule out the possibility that, in this cell system, the observed reduction in L-type Ca^{2+} channel conductance would result from mechanism(s) other than down-expression or mis-membrane-targeting or anchoring of the channel protein. Along this line, Western blot analysis showed that the amount of $Ca_v1.1$ was unchanged in fully matured Cav-3-null mouse muscles (Galbiati *et al.* 2001). These data hence suggest that, unlike in myotubes, the decrease of Ca^{2+} channel conductance in the more differentiated foetal fibers does not result from a reduced density of the protein but is rather primarily due to an altered function of the L-type Ca^{2+} channel associated with the loss of Cav-3. In agreement with this hypothesis, we found that the voltage dependence of the Ca^{2+} current was significantly shifted towards positive membrane potentials in Cav-3^{P104L} expressing foetal fibers but not in myotubes. This result thus strengthens the possibility that the reduced amplitude of $I_{Ca,L}$ in Cav-3^{P104L} expressing cells mainly results from a disruption of the Ca^{2+} channel function in foetal fibers whereas it mainly results from a reduced number of channels in myotubes. Finally, our observation that Cav-3 over-expression in foetal fibers did not have any drastic effect on $I_{Ca,\ L}$ may indicate that under physiological conditions the available amount of endogenous Cav-3 already allows optimal operating of the L-type Ca^{2+} channel.

Our results provide important clues to explain the physio-pathological consequences of Cav-3 deficiency in skeletal muscle. A reduction of function of the DHPR may be associated with muscle weakness since it is directly involved in excitation-contraction coupling (Rios & Pizarro, 1991). This may account for the muscle weakness which characterizes LGMD-1C (Woodman *et al.* 2004). The disease is also associated with progressive muscle wasting (Woodman *et al*. 2004), and, as suspected for a number of muscular dystrophies (Rizzuto & Pozzan, 2003), chronic intracellular Ca^{2+} overload may act in this case as the primary process of necrosis. Along this line, transgenic mice expressing Cav-3^{P104L} were shown to over-produce NO (Sunada *et al.* 2001) which in turn causes a redox-sensitive continuous leak of Ca^{2+} from the sarcoplasmic reticulum (Pouvreau *et al.* 2004b). In this way, the reduction in $I_{Ca,L}$ possibly together with a reduction in the voltage-controlled calcium release in Cav-3 deficient muscle may be seen as a compensatory or protective mechanism to preserve normal Ca^{2+} levels.

References

Balijepalli RC, Foell JD, Hall DD, Hell JW & Kamp TJ (2006). Localization of cardiac L-type Ca^{2+} channels to a caveolar macromolecular signalling complex is required for beta(2)-adrenergic regulation. *Proc Natl Acad Sci USA* **103**, 7500-7505.

Betz RC, Schoser BG, Kasper D, Ricker K, Ramirez A, Stein V, Torbergsen T, Lee YA, Nothen MM, Wienker TF, Malin JP, Propping P, Reis A, Mortier W, Jentsch TJ, Vorgerd M & Kubisch C (2001). Mutations in CAV3 cause mechanical hyperirritability of skeletal muscle in rippling muscle disease. *Nat Genet* **28**, 218-219.

Brazer SC, Singh BB, Liu X, Swaim W & Ambudkar IS (2003). Caveolin-1 contributes to assembly of store-operated Ca^{2+} influx channels by regulating plasma membrane localization of TRPC1. *J Biol Chem* **278**, 27208-27215.

Carozzi AJ, Roy S, Morrow IC, Pol A, Wyse B, Clyde-Smith J, Prior IA, Nixon SJ, Hancock JF & Parton RG (2002). Inhibition of lipid raft-dependent signalling by a dystrophy-associated mutant of caveolin-3. *J Biol Chem* **277**, 17944-17949.

Cohen AW, Hnasko R, Schubert W & Lisanti MP (2004). Role of caveolae and caveolins in health and disease. *Physiol Rev* **84**, 1341-1379.

Couchoux H, Allard B, Jacquemond V, Legrand C & Berthier C (2006). Downregulation of caveolin-3 affects L-type Ca2+ channel functional expression in mouse skeletal muscle. *Biophys J* **90**, B261.

Cognard C, Constantin B, Rivet-Bastide M, Imbert N, Besse C & Raymond G (1993). Appearance and evolution of calcium currents and contraction during the early post-fusional stages of rat skeletal muscle cells developing in primary culture. *Development* **117**, 1153-1161.

Feron O, Belhassen L, Kobzik L, Smith TW, Kelly RA & Michel T (1996). Endothelial nitric oxide synthase targeting to caveolae. Specific interactions with caveolin isoforms in cardiac myocytes and endothelial cells. *J Biol Chem* **271**, 22810-22814.

Flucher BE, Terasaki M, Chin H, Beeler T & Daniels MP (1991). Biogenesis of transverse tubules in skeletal muscle in vitro. *Dev Biol* **145**, 77–90.

Flucher BE, Andrews SB, Fleischer S, Marks AR, Caswell A & Powell JA (1993). Triad formation: organization and function of the sarcoplasmic reticulum calcium release channel and triadin in normal and dysgenic muscle in vitro. *J Cell Biol* **123**,1161-1174.

Franzini-Armstrong C (1991). Simultaneous maturation of transverse tubules and sarcoplasmic reticulum during muscle differentiation in the mouse. *Dev Biol* **146**, 353-363.

Fulizio L, Chiara Nascimbeni A, Fanin M, Piluso G, Politano L, Nigro V & Angelini C (2005). Molecular and muscle pathology in a series of caveolinopathy patients. *Hum Mutat* **25**, 82-89.

Galbiati F, Volonte D, Engelman JA, Scherer PE & Lisanti MP (1999a). Targeted down-regulation of caveolin-3 is sufficient to inhibit myotube formation in differentiating C2C12 myoblasts. Transient activation of p38 mitogen-activated protein kinase is required for induction of caveolin-3 expression and subsequent myotube formation. *J Biol Chem* **274**, 30315-30321.

Galbiati F, Volonte D, Minetti C, Chu JB & Lisanti MP (1999b). Phenotypic behavior of caveolin-3 mutations that cause autosomal dominant limb girdle muscular dystrophy (LGMD-1C). Retention of LGMD-1C caveolin-3 mutants within the golgi complex. *J Biol Chem* **274**, 25632-25641.

Galbiati F, Engelman JA, Volonte D, Zhang XL, Minetti C, Li M, Hou H Jr, Kneitz B, Edelmann W & Lisanti MP (2001). Caveolin-3 null mice show a loss of caveolae, changes in the microdomain distribution of the dystrophin-glycoprotein complex, and t-tubule abnormalities. *J Biol Chem* **276**, 21425-21433.

Hernandez-Deviez DJ, Martin S, Laval SH, Lo HP, Cooper ST, North KN, Bushby K & Parton RG (2006). Aberrant dysferlin trafficking in cells lacking caveolin or expressing dystrophy mutants of caveolin-3. *Hum Mol Genet* **15**, 129-142.

Ishikawa H (1968). Formation of elaborate networks of T-system tubules in cultured skeletal muscle with special reference to the T-system formation. *J Cell Biol* **38**, 51-66.

Jorgensen AO, Shen AC, Arnold W, Leung AT & Campbell KP (1989). Subcellular distribution of the 1,4-dihydropyridine receptor in rabbit skeletal muscle in situ: an immunofluorescence and immunocolloidal gold-labelling study. *J Cell Biol* **109**, 135-147.

Kyselovic J, Leddy JJ, Ray A, Wigle J & Tuana BS (1994). Temporal differences in the induction of dihydropyridine receptor subunits and ryanodine receptors during skeletal muscle development. *J Biol Chem* **269**, 21770-21777.

Luetterforst R, Stang E, Zorzi N, Carozzi A, Way M, & Parton RG (1999). Molecular characterization of caveolin association with the Golgi complex: identification of a cis-Golgi targeting domain in the caveolin molecule. *J Cell Biol* **145**, 1443-1459.

Mallouk N, Jacquemond V & Allard B (2000). Elevated subsarcolemmal Ca^{2+} in mdx mouse skeletal muscle fibers detected with Ca^{2+}-activated K^+ channels. *Proc Natl Acad Sci USA* **97**, 4950-4955.

Martens JR, O'Connell K & Tamkun M (2004). Targeting of ion channels to membrane microdomains: localization of K_V channels to lipid rafts. *Trends Pharmacol Sci* **25**, 16-21.

Matsuda C, Hayashi YK, Ogawa M, Aoki M, Murayama K, Nishino I, Nonaka I, Arahata K & Brown RH Jr (2001). The sarcolemmal proteins dysferlin and caveolin-3 interact in skeletal muscle. *Hum Mol Genet* **10**, 1761-1766.

Minetti C, Sotgia F, Bruno C, Scartezzini P, Broda P, Bado M, Masetti E, Mazzocco M, Egeo A, Donati MA Volonte D, Galbiati F, Cordone G, Bricarelli FD, Lisanti MP & Zara

F (1998). Mutations in the caveolin-3 gene cause autosomal dominant limb-girdle muscular dystrophy. *Nat Genet* **18**, 365-368.

Minetti C, Bado M, Broda P, Sotgia F, Bruno C, Galbiati F, Volonte D, Lucania G, Pavan A, Bonilla E, Lisanti MP & Cordone G (2002). Impairment of caveolae formation and T-system disorganization in human muscular dystrophy with caveolin-3 deficiency. *Am J Pathol* **160**, 265-270.

Nixon SJ, Wegner J, Ferguson C, Mery PF, Hancock JF, Currie PD, Key B, Westerfield M, & Parton RG (2005). Zebrafish as a model for caveolin-associated muscle disease; caveolin-3 is required for myofibril organization and muscle cell patterning. *Hum Mol Genet* **14**, 1727-1743.

Parton RG, Way M, Zorzi N & Stang E (1997). Caveolin-3 associates with developing T-tubules during muscle differentiation**.** *J Cell Biol* **136**, 137-154.

Parton RG & Richards AA (2003). Lipid rafts and caveolae as portals for endocytosis: new insights and common mechanisms. *Traffic* **4**, 724-738.

Pouvreau S, Berthier C, Blaineau S, Amsellem J, Coronado R & Strube C (2004a). Membrane cholesterol modulates dihydropyridine receptor function in mice foetal skeletal muscle cells. *J Physiol* **555**, 365-381.

Pouvreau S, Allard B, Berthier C & Jacquemond V (2004b). Control of intracellular calcium in the presence of nitric oxide donors in isolated skeletal muscle fibres from mouse. *J Physiol* **560**, 779-794.

Rahkila P, Alakangas A, Vaananen K & Metsikko K (1996). Transport pathway, maturation, and targetting of the vesicular stomatitis virus glycoprotein in skeletal muscle fibers. *J Cell Sci* **109**, 1585-1596.

Ralston E & Ploug T (1999). Caveolin-3 is associated with the T-tubules of mature skeletal muscle fibers. *Exp Cell Res* **246**, 510-515.

Rios E & Pizarro G (1991). Voltage sensor of excitation-contraction coupling in skeletal muscle. *Physiol Rev* **71**, 849-908.

Rizzuto R & Pozzan T (2003). When calcium goes wrong: genetic alterations of a ubiquitous signalling route. *Nat Genet* **34**, 135-141.

Romey G, Garcia L, Dimitriadou V, Pincon-Raymond M, Rieger F & Lazdunski M (1989). Ontogenesis and localization of Ca2+ channels in mammalian skeletal muscle in culture and role in excitation-contraction coupling. *Proc Natl Acad Sci USA* **86**, 2933-2937.

Scherer PE & Lisanti MP (1997). Association of phosphofructokinase-M with caveolin-3 in differentiated skeletal myotubes. Dynamic regulation by extracellular glucose and intracellular metabolites. *J Biol Chem* **272**, 20698-20705.

Song KS, Scherer PE, Tang Z, Okamoto T, Li S, Chafel M, Chu C, Kohtz DS & Lisanti MP (1996). Expression of caveolin-3 in skeletal, cardiac, and smooth muscle cells. Caveolin-3 is a component of the sarcolemma and co-fractionates with dystrophin and dystrophin-associated glycoproteins. *J Biol Chem* **271**, 15160-15165.

Sotgia F, Lee JK, Das K, Bedford M, Petrucci TC, Macioce P, Sargiacomo M, Bricarelli FD, Minetti C, Sudol M & Lisanti MP (2000). Caveolin-3 directly interacts with the C-terminal tail of beta -dystroglycan. Identification of a central WW-like domain within caveolin family members. *J Biol Chem* **275**, 38048-38058.

Sunada Y, Ohi H, Hase A, Ohi H, Hosono T, Arata S, Higuchi S, Matsumura K & Shimizu T (2001). Transgenic mice expressing mutant caveolin-3 show severe myopathy associated with increased nNOS activity. *Hum Mol Genet* **10**, 173-178.

Takekura H, Flucher BE & Franzini-Armstrong C (2001). Sequential docking, molecular differentiation, and positioning of T-Tubule/SR junctions in developing mouse skeletal muscle. *Dev Biol* **239**, 204-214.

Tang Z, Scherer PE, Okamoto T, Song K, Chu C, Kohtz DS, Nishimoto I, Lodish HF & Lisanti MP (1996). Molecular cloning of caveolin-3, a novel member of the caveolin gene family expressed predominantly in muscle. *J Biol Chem* **271**, 2255-2261.

Varadi G, Orlowski J & Schwartz A (1989). Developmental regulation of expression of the alpha 1 and alpha 2 subunits mRNAs of the voltage-dependent calcium channel in a differentiating myogenic cell line. *FEBS Lett* **250**, 515-518.

Venema VJ, Ju H, Zou R & Venema RC (1997). Interaction of neuronal nitric-oxide synthase with caveolin-3 in skeletal muscle. Identification of a novel caveolin scaffolding/inhibitory domain. *J Biol Chem* **272**, 28187-28190.

Volonte D, Peoples AJ & Galbiati F (2003). Modulation of myoblast fusion by caveolin-3 in dystrophic skeletal muscle cells: implications for Duchenne muscular dystrophy and limb-girdle muscular dystrophy-1C. *Mol Biol Cell* **14**, 4075-4088.

Wang XL, Ye D, Peterson TE, Cao S, Shah VH, Katusic ZS, Sieck GC & Lee HC (2005). Caveolae targeting and regulation of large conductance Ca^{2+}-activated K^{+} channels in vascular endothelial cells. *J Biol Chem* **280**, 11656-11664.

Way M & Parton RG (1995). M-caveolin, a muscle-specific caveolin-related protein. *FEBS Lett* **376**, 108-112.

Woodman SE, Sotgia F, Galbiati F, Minetti C & Lisanti MP (2004). Caveolinopathies: mutations in caveolin-3 cause four distinct autosomal dominant muscle diseases. *Neurology* **62**, 538-543.

Acknowledgments

We are very grateful to Dr R.G. Parton (University of Queensland, Australia) for the gift of the wild type and P104L caveolin cDNAs and to Dr L.E. Espinosa (University of Marseille, France) for his expert advice and help regarding image analysis. This work was supported by grants from CNRS, Agence Nationale de la Recherche, Université Lyon 1 and Association Française contre les Myopathies.

Figure Legends

Figure 1. Cav-3^{P104L}-YFP expression leads to the loss of Cav-3 in primary cultured myotubes.

A, in control myotubes, Cav-3 immunolabeling strongly outlines the surface plasma membrane. It localizes as well intracellularly in small dot-shaped clusters (arrowheads) as best seen on the partial 2X enlargement (inset). *B*, Cav-3^{P104L}-YFP accumulates preferably around the nuclei in vesicular structures (top image). Cav-3 immunolabeling is dramatically decreased, if not totally absent, in the Cav-3^{P104L}-YFP-expressing myotube (arrow) whereas membrane staining is seen at an extremity of a nearby non-transfected myotube (bottom image). Scale bars = 10 µm.

Figure 2. $I_{Ca,\,L}$ is reduced in Cav-3^{P104L}-expressing primary cultured myotubes.

A, representative currents elicited by applying 500 ms-lasting voltage pulses from a holding potential of –80 mV to the indicated values in the two kinds of cells. *B*, mean current-voltage relationships established for the fast transient current ($I_{Ca,\,T}$) and for the slow activating current ($I_{Ca,\,L}$) in 40 control and 21 Cav-3^{P104L}-expressing myotubes. *C*, mean current-voltage relationships of isolated $I_{Ca,\,L}$ on the same control and mutant myotubes. The superimposed curves were calculated using the mean parameters obtained from fitting the voltage dependence in each fibre (see text for details).

Figure 3. Double immunolabeling reveals a strong colocalization of Cav-3 and $Ca_v1.1$ in primary cultured myotubes.

Cav-3 (red) and $Ca_v1.1$ (green) strongly colocalizes as clearly shown on the merged images. The colocalization is particularly pronounced at the surface plasma membrane, where both proteins accumulate (arrows).

Additionally, the $Ca_v1.1$ labelling appears characteristically concentrated within internal punctate structures distributed rather uniformly throughout the cell and likely belonging to the developing T-tubule network. Cav-3 labelling appears generally weaker in this internal

compartment except for specific areas, where it co-localizes with $Ca_v1.1$ (arrowheads). Scale bar = 10 µm.

Figure 4. Localization and labelling intensity of $Ca_v1.1$ are altered in Cav-3^{P104L}-expressing myotubes.

A, in this representative Cav-3^{P104L}-YFP expressing myotube (green), $Ca_v1.1$ labelling (red) appears much dimmer as compared to the non-transfect neighbouring myotubes and is in addition partly redistributed to the perinuclear region where it colocalizes with Cav-3^{P104L}, as shown on the merged images (arrow). Scale bar = 10 µm. *B*, numerical image analysis of $Ca_v1.1$ labelling intensity. Field-specific analysis was performed on confocal Z-stacks by measuring $Ca_v1.1$ immunoreactivity of control myotubes (Ct) and Cav-3^{P104L}-expressing myotubes (P104L) present on a same image. Mean labelling intensity appeared to be reduced by a mean 66% percent in Cav-3^{P104L}-expressing myotubes ($P < 0.0001$).

Figure 5. In foetal fibers, $I_{Ca,\ L}$ is also altered by Cav-3^{P104L} expression but is not affected by WT Cav-3 expression.

A, immunolocalization of Cav-3 in foetal fibers expressing Cav-3^{P104L}-YFP (top panel) and YFP-tagged wild type Cav-3 (WT-Cav-3, bottom panel). YFP-tagged Cav-3^{P104L} preferentially accumulates around nuclei (asterisks), as shown in this representative transfected fibre in which almost no endogenous Cav-3 is revealed by anti-Cav-3 antibody immunolabeling. Conversely, immunolabeling clearly revealed endogenous Cav-3 in the nearby non-transfected fibre. YFP-tagged wild type Cav-3 appears concentrated at the surface plasma membrane as well as in discrete intracellular clusters, where it is also detected by immunolabeling. Scale bar = 20 µm, applies to all images. *B*, representative $I_{Ca,\ L}$ recordings, elicited by applying 500 ms-lasting voltage pulses from a holding potential of –80 mV to a potential of +30mV. *C*, left panel, mean current-voltage relationships established for the current in 31 control, 8 Cav-3^{P104L} and 16 WT Cav-3 expressing foetal fibers. The superimposed curves were calculated using the mean parameters obtained from fitting the voltage dependence in each fibre (see text for details). The right panel presents

the mean normalized conductance-voltage relationship in control (n=31) and Cav-3^{P104L} expressing (n=8) foetal fibers.

Figure 1

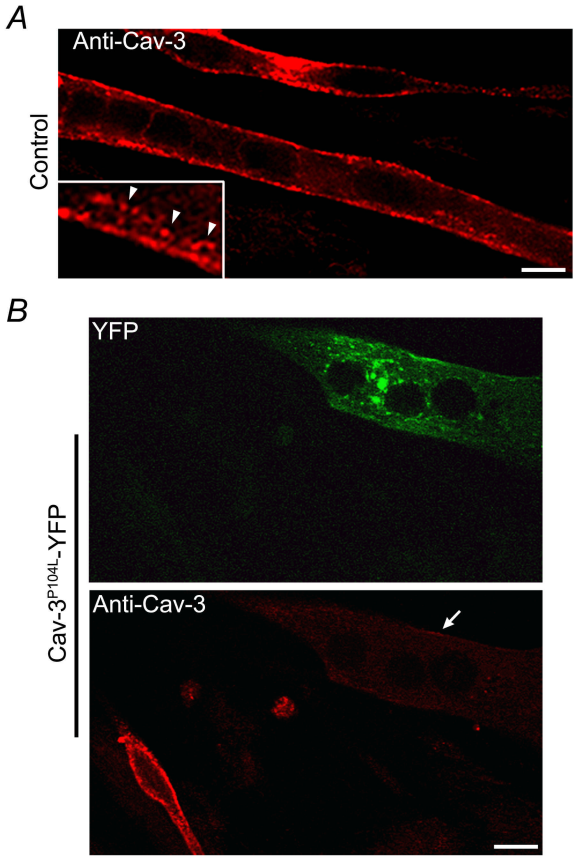

Figure 2

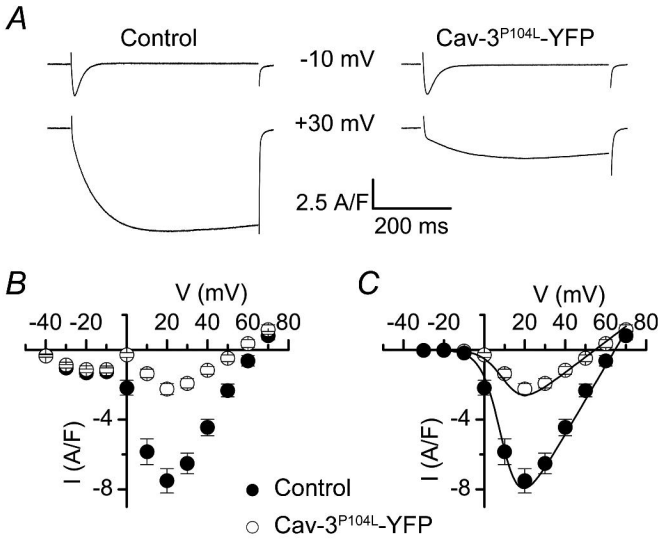
A
Control
Cav-3P104L-YFP
-10 mV
+30 mV
2.5 A/F
200 ms
B
V (mV)
-40 -20 20 40 60 80
-4
-8
I (A/F)
C
V (mV)
-40 -20 20 40 60 80
-4
-8
I (A/F)
Control
Cav-3P104L-YFP

Figure 3

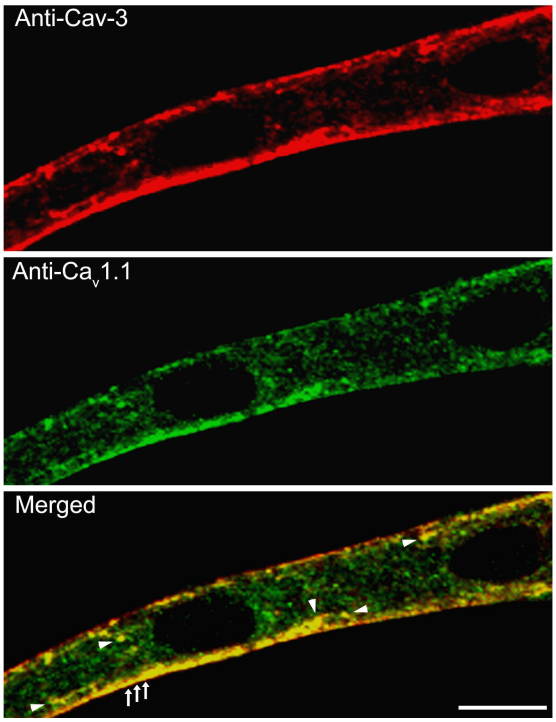

Figure 4

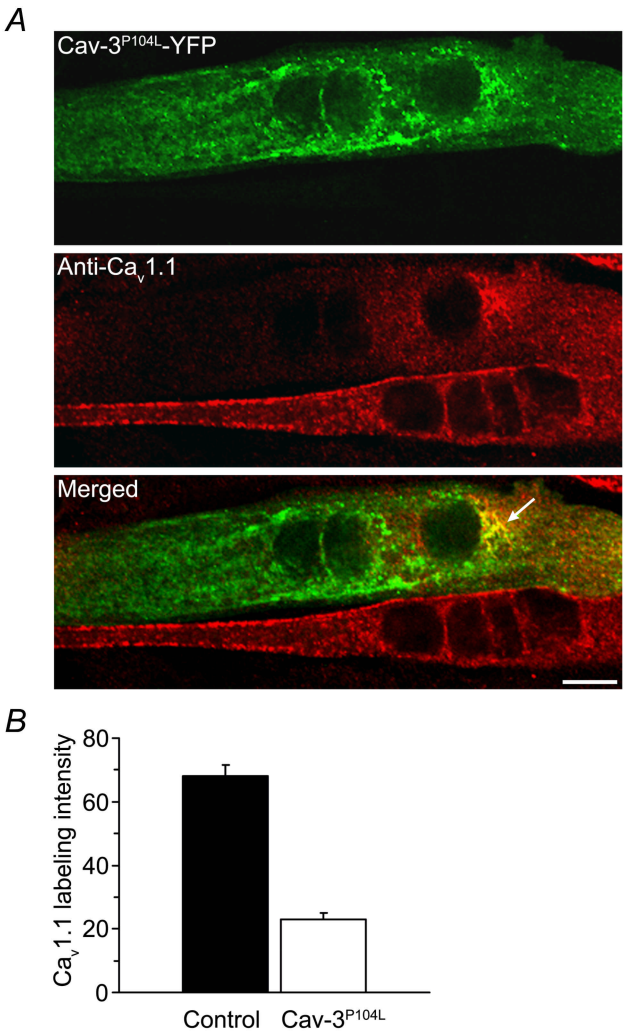
A
Cav-3P104L-YFP
Anti-Cav1.1
Merged
B
Cav1.1 labeling intensity
80
60
40
20
0
Control
Cav-3P104L

Figure 5

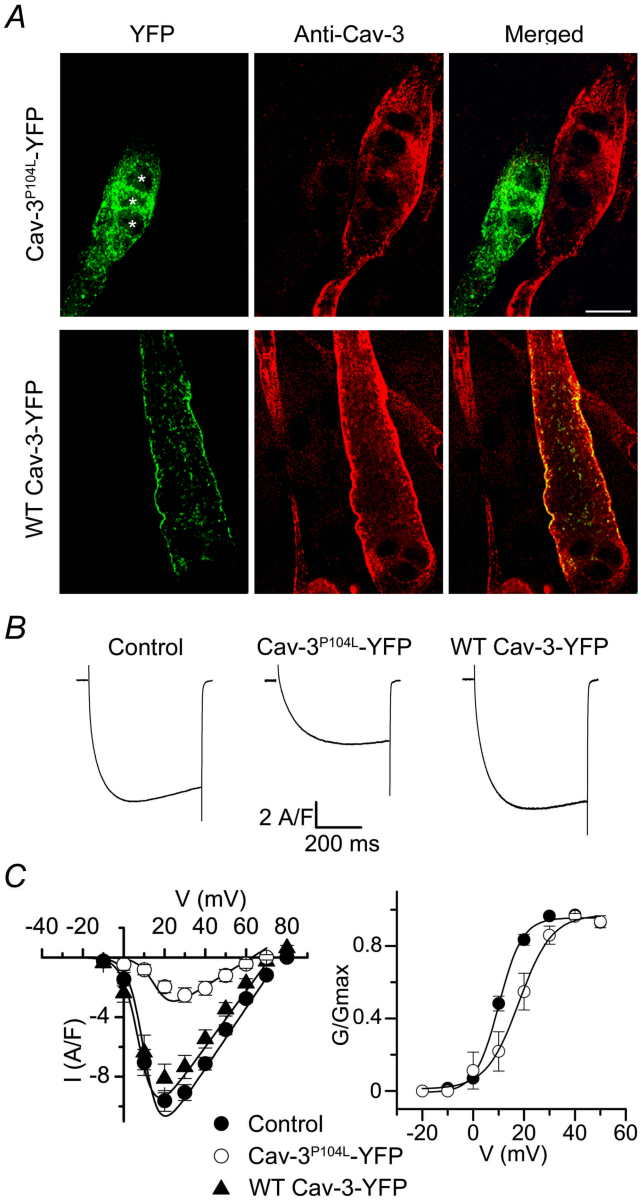
A
YFP
Anti-Cav-3
Merged
Cav-3P104L-YFP
WT Cav-3-YFP
B
Control
Cav-3P104L-YFP
WT Cav-3-YFP
2 A/F
200 ms
C
V (mV)
-40 -20
20 40 60 80
-4
-8
I (A/F)
0.8
0.4
0
G/Gmax
-20 0 20 40 60
V (mV)
Control
Cav-3P104L-YFP
WT Cav-3-YFP